Chem

CellPress

Article

2D $Ti_3C_2T_z$ MXene Synthesized by Water-free Etching of Ti_3AlC_2 in Polar Organic Solvents

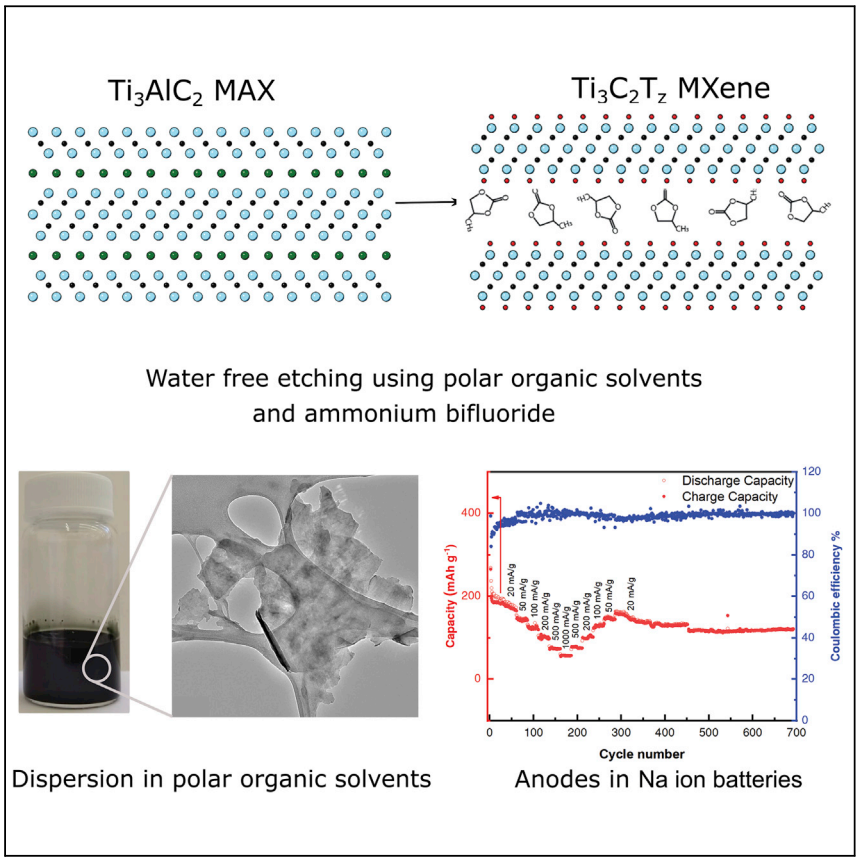

The majority of etching methods for synthesizing MXenes use water as the main solvent, which in turn limits direct use of MXenes in water-sensitive applications. In this work, we show that it is possible to etch, and delaminate, MXenes in the absence of water by using organic polar solvents and ammonium dihydrogen fluoride. We also demonstrate that electrodes made from $Ti_3C_2T_z$ etched in propylene carbonate, resulted in Na-ion battery anodes with double the capacity to those etched in water.

Varun Natu, Rahul Pai, Maxim Sokol, Michael Carey, Vibha Kalra, Michel W. Barsoum

barsoumw@drexel.edu

HIGHLIGHTS

Water-free synthesis of MXenes using polar solvents and NH_4HF_2 solutions

MXene synthesized in propylene carbonate show enhanced performance in Na-ion batteries

If synthesized in a glove box, the MXenes terminations are majorly fluorine

Natu et al., Chem 6, 616–630
March 12, 2020 © 2020 Elsevier Inc.
https://doi.org/10.1016/j.chempr.2020.01.019

Chem

CellPress

Article

2D $Ti_3C_2T_z$ MXene Synthesized by Water-free Etching of Ti_3AlC_2 in Polar Organic Solvents

Varun Natu,[1] Rahul Pai,[2] Maxim Sokol,[1] Michael Carey,[1] Vibha Kalra,[2] and Michel W. Barsoum[1,3,*]

SUMMARY

The first MXene discovered, $Ti_3C_2T_z$, was synthesized by etching of the parent MAX phase, Ti_3AlC_2, in a solution of concentrated hydrofluoric acid. Since then, several other ways of synthesizing MXenes have been reported, such as electrochemical etching in various electrolytes, high-temperature alkali treatment, molten salt synthesis, etc. The majority of these etching methods, however, use water as their main solvent, limiting direct use of MXenes in water-sensitive applications. In this work, we show that it is possible to etch, and delaminate, MXenes in the absence of water, by using organic polar solvents in the presence of ammonium dihydrogen fluoride. We further show that by using this etching method, it is possible to obtain $Ti_3C_2T_z$ flakes rich in fluorine terminations. We also demonstrate that electrodes made from $Ti_3C_2T_z$ etched in propylene carbonate resulted in Na-ion battery anodes with double the capacity to those etched in water.

INTRODUCTION

Since the discovery of 2D titanium carbide ($Ti_3C_2T_z$) MXene in 2011 by Naguib et al.,[1] nearly 30 new MXenes have been discovered so far and more are being routinely discovered.[2] Owing to their chemical diversity, hydrophilicity, 2D morphology, and metallic conductivity, MXenes have shown promise in various applications like energy storage,[3] catalysts for hydrogen evolution reactions,[4] gas sensing,[5] water desalination,[6] reinforcement in polymer composites,[7] and electromagnetic interference (EMI) shielding,[8] among many others.

MXenes have a general formula $M_{n+1}X_nT_z$ and are so called because they are derived by etching the A atomic layers from the parent MAX ($M_{n+1}AX_n$) phase, where M stands for an early transition metal, A is mostly a group 13 or 14 element, and X stands for C, N, or B.[9,10] The -ene suffix was added to make the connection to other 2D materials, such as graphene, silicene, etc. The T_z in the chemical formula stands for the various –O, –OH, and –F surface terminations that replace the Al layers upon etching.[1] The first MXene discovered was $Ti_3C_2T_z$, obtained by etching Ti_3AlC_2 powders in concentrated hydrofluoric (HF) acid.[2] In general, multilayered (ML) MXenes etched with HF cannot be delaminated to form stable, high concentration colloids in water. To disperse these MLs, they typically have to be intercalated with organic molecules like dimethyl sulfoxide (DMSO), tetramethylammonium hydroxide (TMAOH), tetrabutylammonium hydroxide (TBAOH), etc.[11]

To overcome this multistep delamination process and to avoid the use of hazardous HF, Ghidiu et al. used an etching solution comprised of lithium fluoride (LiF) and hydrochloric acid (HCl) that formed HF *in situ*. In this system, the Li ions are intercalated

The Bigger Picture

The 2D transition metal carbides and nitrides called MXenes are generally synthesized top down by exposing the parent MAX phase to fluoride-ion-containing acids. This acid treatment selectively etches out only the A-atomic layers from the MAX phase and results in 2D MXene sheets. To date, the most common solvent used for this acid treatment is water, rendering the use of MXenes in water-sensitive applications difficult. In this work, we show that it is possible to etch the MAX phase in a solution of a polar organic solvent and ammonium dihydrogen fluoride and obtain F-terminated MXenes without the use of water. This opens avenues for use of MXenes in numerous water-sensitive applications such as energy storage, polymer composites, supports for quantum dots, etc.

during etching, which, when the pH approaches neutral, results in spontaneous delamination.[12] More recently, Li et al. synthesized MXene by etching Ti_3AlC_2 using a high-temperature hydrothermal approach in a high pH sodium hydroxide (NaOH) solution.[13] Yang et al. showed that it was possible to electrochemically etch MAX phases into MXenes in an ammonium chloride and TMAOH electrolyte.[14] These two methods showed, for the first time, F-free synthesis of MXene. More recently Li et al. showed a one-step molten salt ($ZnCl_2$) etching of MAX phases to synthesize –Cl terminated MXenes.[15] Delamination of these –Cl terminated MXenes to form a stable colloid of single to few layers of MXene has not been reported, possibly because of the absence of intercalated cations and/or the absence of –O/–OH terminations. The latter are typically associated with colloidal stability after delamination.[11,16]

In short, most near-ambient temperature synthesis methods, known to date, use water as the main solvent. Using water as a solvent, however, poses problems when incorporating MXenes in some applications. For example, certain polymerization reactions are hampered by the presence of water, making synthesis of *in situ* polymerized nanocomposites reinforced with MXenes difficult.[17,18] The synthesis of specific quantum dots on MXenes sheets might also not be possible, again, because of the presence of water.[19] Most importantly, it is well established that even trace amounts of water in Li or Na ion batteries using organic electrolytes can negatively impact their performance, making vacuum annealing of MXene anodes mandatory before cell assembly.[20]

Herein, we show that it is possible to etch, and delaminate, Ti_3AlC_2 in a variety of organic solvents in the presence of ammonium dihydrogen fluoride, NH_4HF_2 (Figure 1). We further show that the $Ti_3C_2T_z$ synthesized in propylene carbonate (PC) exhibit nearly double the capacity compared to the same MXene etched in water when tested as electrodes in Na-ion batteries (SIB) in a PC-containing electrolyte.

RESULTS AND DISCUSSION

Figure 2A depicts the X-ray diffraction (XRD) patterns of as-etched MXene just before washing, while Figure 2C depicts the XRD patterns after delamination followed by filtering and grinding. Figures 2B and 2D focus on the low angle region. Henceforth, to denote the MXene etched using a particular solvent, the prefix of the solvent abbreviation is added before the acronym, MX. For example, samples synthesized in PC are labeled PC-MX, those in acetonitrile, ACN-MX, etc. The sequence of the patterns is the same in all 4 panels with acetonitrile (ACN)-MX (top, yellow), dioxane (DXN)-MX (second, purple), N,N-dimethylformamide (DMF)-MX (third, green), DMSO-MX (fourth, blue), N-methyl-2-pyrrolidone (NMP)-MX (fifth, red), and PC-MX (last, black). Figure 2B shows highly expanded basal spacings, which can be determined from the position of the 002 peak present near 2° 2θ[1,21] for all samples, except DMSO-MX, for which the 002 peak was around 4.2° 2θ. The d-spacings calculated are listed in Table 1. To confirm the d-spacings calculated from XRD, the d-spacings of a representative PC-MX sample (before washing) were also measured in a transmission electron microscopy (TEM). As shown in Figure S1, and not too surprisingly, the d-spacing from the micrograph (38.6 Å) is in good agreement with the spacing obtained for XRD, viz. 39 Å.

The d-spacings, between 21–51 Å, measured herein, are significantly higher than the d-spacing of 12.3 Å obtained by Halim et al., who etched Ti_3AlC_2 thin films in NH_4HF_2 and water.[22] This suggests that during etching in organic solvents, the interlayer space is most probably occupied by NH_4^+ cation complexes associated with organic solvent molecules and not bare cations.

[1]Department of Materials Science and Engineering, Drexel University, Philadelphia, PA 19104, USA

[2]Department of Chemical and Biological Engineering, Drexel University, Philadelphia, PA 19104, USA

[3]Lead Contact

*Correspondence: barsoumw@drexel.edu

https://doi.org/10.1016/j.chempr.2020.01.019

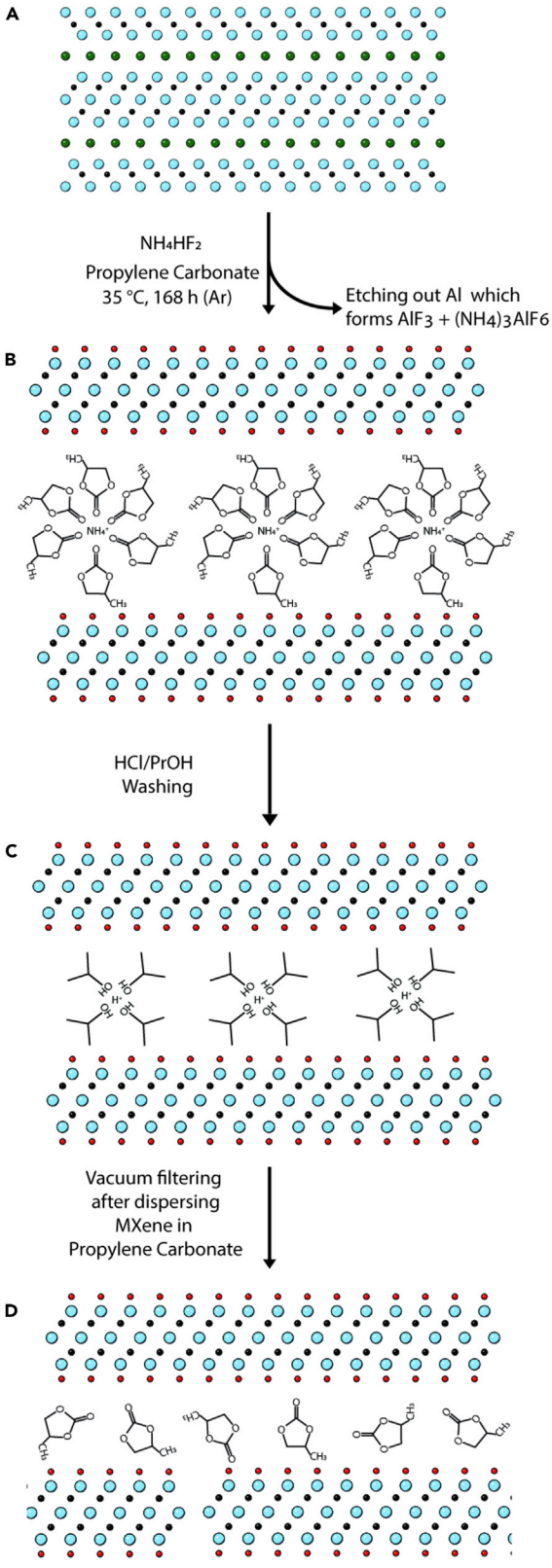
A
NH4HF2
Propylene Carbonate
35 °C, 168 h (Ar)
Etching out Al which
forms AlF3 + (NH4)3AlF6
B
HCl/PrOH
Washing
C
Vacuum filtering
after dispersing
MXene in
Propylene Carbonate
D

Figure 1. Schematic of Etching and Washing Steps

(A) Starting Ti_3AlC_2 phase, (B) after etching with NH_4HF_2 in organic solvent, (C) after washing in HCl/2-propanol mixture, and (D) final state after filtering. Note what is depicted between the layers is only shown for the sake of the schematic and in no way should be construed to be what is actually occurring.

As no information was found in the literature about the solvation of ammonium cations by various organic molecules, it is difficult to explain the small differences observed in d-spacings, especially in the DMSO-MX case, where the d-spacing was found to be smaller than in all other cases (Table 1). In their recent work, Verger et al. showed that when etching Ti_3AlC_2 phase in LiF and HCl solutions, the d-spacing increased from 14 Å (≈ 6.3° 2θ) to 16.5 Å (≈ 5.5° 2θ) as the pH increased, due to washing, from 1 to 5. The authors attributed this increase to the hydration of intercalated cations as the pH approached 7.[23] This does not seem to be the case here, where sharp high-intensity peaks at low angles (<3° 2θ) are seen in the XRD patterns, indicating several solvent layers or highly solvated ammonium cations between the MXenes layers are present, even before washing. This result highlights the significant differences in the etching and/or intercalation processes when etching in water versus etching in organic solvents.

The small peak around 9° 2θ, seen in the ACN-MX, DMF-MX, DXN-MX, and PC-MX samples, corresponds to leftover Ti_3AlC_2 powder that was not completely etched (Figure 2A). Also, peaks of AlF_3 and $(NH_4)_3AlF_6$ are seen in MXene patterns before washing (Figure 2A). These peaks result from the salts formed when the Al is etched out.

Figures 2C and 2D show XRD patterns of filtered films after grinding. Only peaks corresponding to MXene are seen in all but the DXN-MX sample (Figure 2D). The small peak around 9° 2θ, seen only in the latter, is again due to unetched or partially etched MAX particles.

It is important to note that, because the organic solvents used in this work have low solubilities for the Al-salts formed during etching, they could not be washed away without the use of acidic propanol. Somewhat surprisingly, after washing, the d-spacings reduce significantly and range between 13.5–21 Å depending on the solvent used (column 3, Table 1). The most probable cause for this reduction is the exchange of ammonium cations with protons present in the acidic propanol. This is consistent with earlier work on cation exchange in MXenes etched in water[24] but is observed here, to occur for the first time, in multiple polar solvents other than water. Interestingly, the d-spacing of the DMSO-MX sample remains constant at ≈ 21 Å, before and after washing, implying no cationic exchange in this case.

When solvent exchange was carried out in kaolinite clays, it was found that upon interaction with DMF, NMP, or ACN, there is 4–5 Å increase in the d-spacing compared to dry kaolinite.[25,26] This might explain the ≈ 4.5 Å increase in the washed ACN-MX, NMP-MX, and DMF-MX compared to HF-only etched $Ti_3C_2T_z$ MLs (d ≈ 9.8Å).[1,27] The latter can be considered a "dry" $Ti_3C_2T_z$ since we now know that in that case no water is intercalated between the layers. It follows that the ≈ 4.5 Å increase most probably reflects the intercalation of the organic solvent between the MXene layers. Along the same lines, the 14 Å d-spacing in the washed PC-MX matches the work of Collini et al. on electrophoretic deposition of $Ti_3C_2T_z$ in a PC electrolyte,[28] again confirming the presence of PC between the layers.

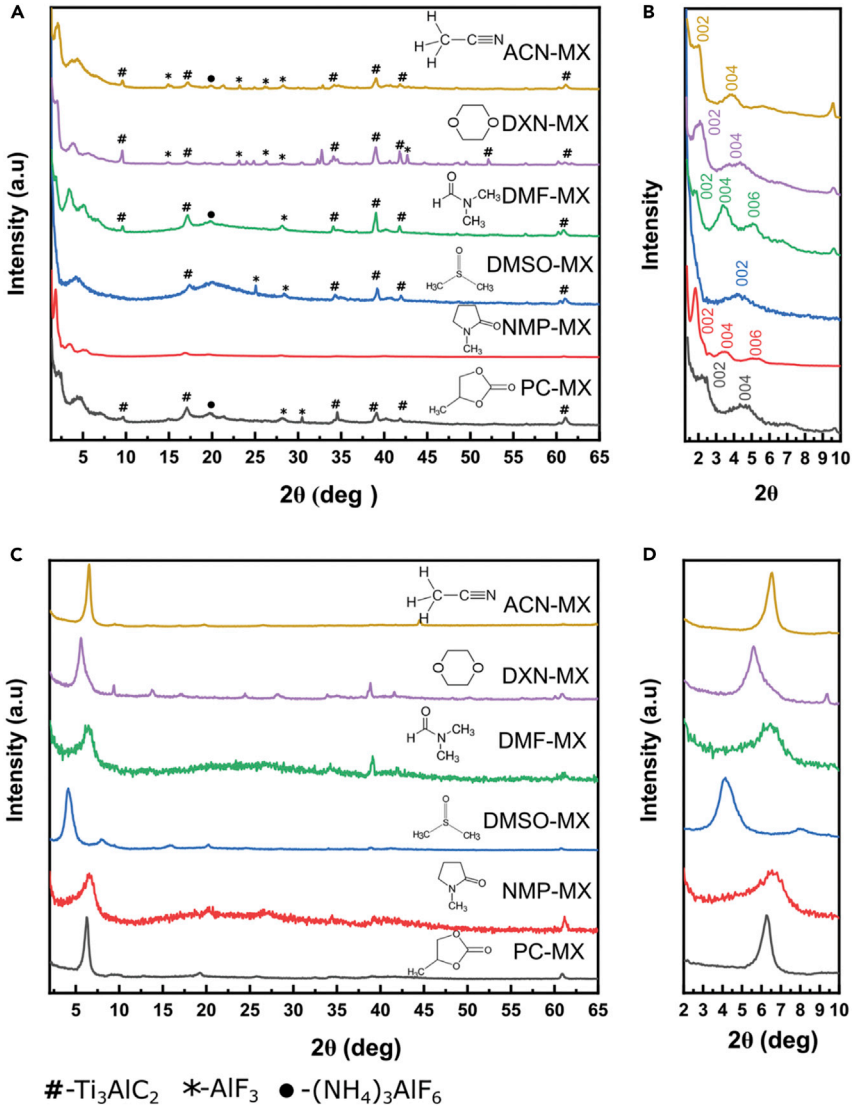

Figure 2. XRD Patterns of $Ti_3C_2T_z$, Synthesized in Organic Solvents

(A) Before washing, right after etching; (B) same as (A) but focused on 1.2°–10° 2θ region to clearly depict the 002 peaks; (C) after washing, drying, and grinding of filtered films; (D) Same as (C) but focused on low angles. Patterns are shifted vertically for clarity. The molecular structure of the organic solvents used are shown right above the corresponding XRD pattern. Sequence of XRD patterns is the same in all 4 panels and corresponds to ACN- (top, yellow), DXN- (second, purple), DMF- (third, green), DMSO- (fourth, blue), NMP- (fifth, red), and PC-MX (sixth, black).

Figure S3 presents the XRD patterns of the samples that were first etched in HF and water and then solvent exchanged for a week. Figure S3 shows, that except for DMSO, no other solvent intercalated between the MXene sheets. It follows that our etching method can be used to intercalate MLs with multiple layers of organic solvents and not just DMSO.

Figure 3A shows typical SEM micrographs of a PC-MX sample after washing but before delamination. The accordion-like morphology is typical of etched Ti_3AlC_2 powders and further confirms the successful synthesis of $Ti_3C_2T_z$.[1,12] Similar morphologies were also observed in MXenes synthesized in the other solvents

Table 1. Interlayer d-Spacings (= c/2, Where c Is the Lattice Parameter) of Samples Calculated from the Position of 002 Peak Before and After Washing

Sample	d-spacing, Å, (2θ)	
	Before Washing	After Washing
ACN-MX	45.0 (2.0)	13.5 (6.5)
DXN-MX	41.9 (2.1)	15.7 (5.6)
DMF-MX	50.7 (1.7)	13.5 (6.5)
DMSO-MX	21.1 (4.2)	21.2 (4.1)
NMP-MX	48.7 (1.8)	13.5 (6.5)
PC-MX	39.0 (2.2)	14.0 (6.3)

The 2nd column lists the d-spacings in Å, before washing right after etching; last column lists the values after drying and grinding the filtered films obtained after washing. Values in bracket show 2θ angle at which the 002 peak is located.

(Figures S2A–S2E). Figure 3B is a typical TEM micrograph of $Ti_3C_2T_z$ flakes obtained after sonicating the multilayers. The selected area diffraction (SAED) pattern (Figure 3C) further confirms the presence of $Ti_3C_2T_z$ monolayers. There is, thus, little doubt that it is possible to delaminate $Ti_3C_2T_z$ MLs using the procedure outlined herein. We note, in passing, that there is little evidence for TiO_2 nanoparticles on the surface of the flakes, that are sometimes seen when the etching is carried out in water. A picture of the PC-MX colloidal suspension is shown in Figure 3D.

To estimate the solid content of the colloidal suspensions, after delamination, the powders were dried under vacuum for 12 h. The highest concentration colloids are obtained in PC-MX, DMF-MX, DMSO-MX, and NMP-MX samples with values between 0.7–1 mg/mL. These numbers are similar to the ones reported by Collini et al. and Maleski et al.[28,29] For DXN-MX and ACN-MX, the concentrations obtained were significantly lower, with values ranging from 0.1–0.3 mg/mL. Since all the solvents used here have higher molecular weights than water, any residual solvents in the films might have a larger impact on the concentration measurements than those etched in water. Therefore, more work is needed to ensure that the drying of the MXene films, intercalated with high boiling point (BP) solvents like PC (BP 240°C), DMSO (BP 189°C), etc., is complete. Said otherwise, the concentrations reported above may be overestimated.

The zeta potential of the PC-MX sample was measured and was found to be -40 ± 5 mV. This value is close to that of $Ti_3C_2T_z$ flakes synthesized in HF and water mixtures[16] and is most probably responsible for the high colloidal stabilities observed. The interaction of MXene surface terminations with different solvents has been studied in detail by Maleski et al., where the authors show the correlation between various Hanson and Hillebrand parameters of different solvents and the colloidal stability of MXene. There is no reason to believe that similar interactions are not occurring here.

The X-ray photoelectron spectroscopy (XPS) photoemission spectra of the Ti 2p region of PC-MX filtered films are depicted in Figure 4. The curves were fit using the procedure outlined by Halim et al.[30] but with binding energy (BE) that are shifted (see below). The red, blue, and green peaks are ascribed to the +1, +2, and +3 oxidation states of Ti, when bonded to –O/–OH groups, respectively. The yellow peaks correspond to the –F terminations and are at a higher BE compared to the –O/–OH terminations because of bonding with highly electronegative F atoms. By quantifying the number of surface terminations present, it is clear that the freshly

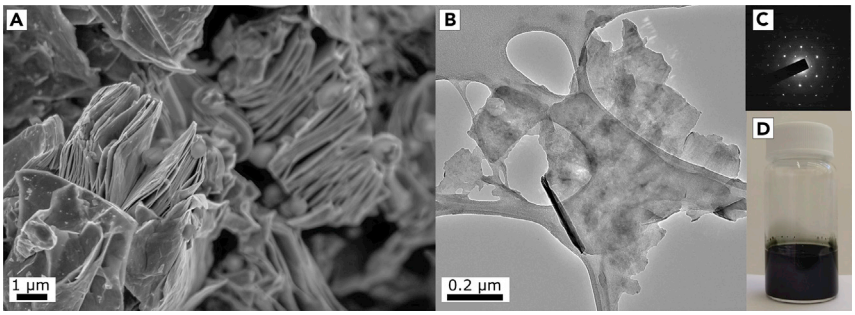

Figure 3. PC-$Ti_3C_2T_z$ Sample
(A) Typical SEM micrograph; (B) TEM micrographs of delaminated sheets; (C) SAED pattern obtained from flakes shown in (B); (D) photograph of PC-MX colloidal suspension.

synthesized MXene is mostly (≈ 70%) F-terminated and the remaining 30% are –O/–OH terminations. As far as we are aware, this is the highest fraction of F-terminations ever reported. The 30% –O/–OH terminations, most probably, result from the brief exposure to air and/or the dissociation of propanol during washing, which was carried out outside the glovebox.

It is fairly well established in the MXene literature that F-terminations are less favored than their O counterparts, and upon long term exposure to ambient atmosphere, the F-terminations are replaced by –O/–OH terminations.[30] To confirm this conclusion, we rescanned the sample used to obtain the results shown in Figure 4A, after exposure to the ambient atmosphere for 12 h. As seen in Figure 4B, the atomic fraction of F-terminations drops to just 0.07. Furthermore, to back this important conclusion, we compared the global atomic percentages calculated by measuring the total area under the photoemission spectra—normalized by the Ti concentration—of the different elements, before and after exposure to air. From the results listed in Table S1, it is obvious that the overall F-content decreases by a factor of almost 2 upon exposure to the atmosphere. The loss of F-signal is consistent with our assigning the peak around 459 eV to F. Had it been due to TiO_2, its intensity would have, if anything, increased upon exposure to air rather rather than decreasing as observed. The details of the fittings and the peak positions are given in Table 2.

Also, listed in Table 2 are the results of Halim et al.[30] for comparison purposes. A perusal of the two sets of results makes it clear that the BEs of the Ti and F peaks determined herein are different from previous ones.[30] For example, the lowest BE Ti 2p peak associated with Ti–C has been previously reported at 455.0 eV[30]; here, it appears at 454.4 eV. The Ti-F peak has been previously reported at 460.0 eV; here, it appears at 459.0 eV. Similarly, the F 1s signal is found at 686.5 eV, (Figures S5A and S5B; Table S2) while in previous work, it was at 685.0 eV. These shifts are not small. It was tempting to assign the differences to an incorrect zero-point calibration, but the BE of the C 1s peak is at 282 eV (Figures S5C and S5D; Table S2) viz. where it has always been reported to be. It follows that for reasons that are not clear, and beyond the scope of this work, the presence of large fractions of F-terminations influences the BE of at least the Ti and F atoms, but not the C. What is indisputable here, however, is that in this work, a Ti-F peak appears at 459.0 eV (Figure 4) and that exposure to the ambient reduces the F-content (compare Figures S5A and S5B; Table S1).

To demonstrate that etching in organic solvents can enhance MXene performance in some applications, we tested the PC-MX films as anodes in a Na-ion battery. This

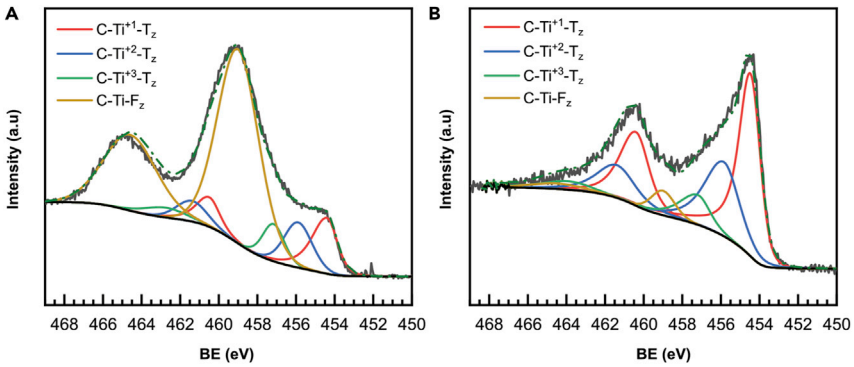

Figure 4. XPS of Ti 2p Region for PC-MX Samples

(A) Immediately after etching and washing and, (B) after 12 h of exposure to the ambient atmosphere.

specific MXene sample was chosen because PC between the MXene layers may form a continuous interface between the MXene layers and the PC/EC electrolyte used in the Na-ion battery, possibly allowing easier diffusion of Na^+ into the electrodes. To investigate Na-ion insertion-extraction behavior in PC-MX films, cyclic voltammetry (CV) and galvanostatic charge-discharge tests were performed (Figure S4). The CV curves in Figure 5A of the PC-MX electrode in the Na-ion electrolyte are similar to other MXene electrodes reported in the literature.[3,31,32] In the first cathodic scan, one irreversible reductive peak occurs at higher potentials (~0.5 V), which is known to reflect the decomposition of the electrolyte and the formation of a solid electrolyte interphase (SEI) on the anode surface. Additionally, Na-ion insertion-extraction behavior is observed with a sharp cathodic peak in the lower potential region (0−0.2 V), and a broad anodic peak (0–1 V) can be clearly observed. These peaks are ascribed to Na-intercalation into the conducting carbon added into the electrodes, but the capacity contribution from this conducting carbon is negligible as shown in our earlier reports.[3] A pair of small and broad redox peaks can be detected in a wide potential range of 1.2–2.5 V, which can be ascribed to the surface redox reactions on the MXene surface. From the above discussion, we can infer that the working mechanism of PC-MX anode takes place in two stages. The reaction occurring in the higher potential (1.2–2.5 V) range is attributed to the pseudocapacitive and/or surface redox charge transfer processes on the MXene surfaces, while the reaction occurring in the narrow, low potential range (0–0.2 V) is ascribed to Na-ion insertion-extraction in the conductive carbon additive. The slight pseudocapacitive and/or surface redox behavior observed in PC-MX is attributed to Na insertion in host stacked MXene and simultaneous charge transfer via a change in Ti oxidation states to maintain charge neutrality.[33] Since, in delaminated PC-MX, stacking of the layers is weak and random due to which the pseudocapacitive and/or surface redox peaks are smaller in area, compared to reports where multilayered MXene was used.[34,35] Additionally, Lin et al. found that pseudocapacitive contribution from the –F and –OH surface groups is negligible when MXene supercapacitors were tested in aprotic solvent electrolytes and the minor peaks around 1.0–1.5V were attributed to cation insertion between the weakly stacked MXene layers.[36] Because PC is also an aprotic solvent, we can assume similar charge storage mechanism, which can also help explain the minor peaks at high voltages (1.2–2.5 V) in our CV curves. After the first few cycles, the CV curves almost overlap, suggesting the capacity decay mainly occurs in the initial cycles, and subsequently the electrode shows good Na ion insertion-extraction stability with minimal pseudocapacitive/surface redox behavior.

Table 2. Summary of XPS Ti $2p_{3/2}$ Peaks Shown in Figure 4 for PC-MX Samples Right after Washing and after 12 h Exposure to Ambient Atmosphere

Sample	BE (eV)	FWHM (eV)	Fraction	Assigned to
PC-MX (Fresh)	454.4 (460.5) 455.9 (461.4) 457.2 (462.7) 459.0 (464.6)	1.2 (1.3) 1.7 (1.9) 1.3 (2.5) 2.5 (3.2)	0.13 0.11 0.07 0.69	C-Ti^{+1}-T_z C-Ti^{+2}-T_z C-Ti^{+3}-T_z C-Ti-F_z
PC-MX (after Exposure to Air for 12 h)	454.4 (460.5) 455.9 (461.4) 457.2 (462.7) 459.0 (464.6)	1.2 (1.6) 1.7 (2.3) 1.4 (2.7) 1.5 (3.1)	0.51 0.30 0.11 0.07	C-Ti^{+1}-T_z C-Ti^{+2}-T_z C-Ti^{+3}-T_z C-Ti-F_z
Water/HF-Etched $Ti_3C_2T_z$ (Values from Halim Et Al.[30])	455.0 (461.2) 455.8 (461.3) 457.2 (462.9) 458.6 (464.2) 459.3 (465.3) 460.2 (466.2)	0.8 (1.5) 1.5 (2.2) 2.1 (2.1) 0.9 (1.0) 0.9 (1.4) 1.6 (2.7)	0.28 0.30 0.32 0.02 0.03 0.05	C-Ti^{+1}-T_z C-Ti^{+2}-T_z C-Ti^{+3}-T_z TiO_2 $TiO_{2-x}F$ C-Ti-F_z

Numbers in brackets in column 2 are peak locations for Ti $2p_{1/2}$ and full width at half maximum (FWHM) values for Ti $2p_{1/2}$ peaks are in brackets in column 3. Also listed in the last rows are BE for HF etched $Ti_3C_2T_z$ as reported by Halim et al.[30] for easy comparison.

Figure 5B depicts the cycling performance of PC-MX, as a function of current density starting at 20 $mA \cdot g^{-1}$. The capacity was initially found to be around 200 $mAh \cdot g^{-1}$, and with cycling, it stabilized to around 160 $mAh \cdot g^{-1}$, which is one of the highest capacity values achieved for non-templated pure $Ti_3C_2T_z$ (Table S3), proving that indeed etching and washing in organic solvents can nearly double the capacity of Na MXene anodes.[34] The fact that nearly 40% of the original capacity is retained even when the current is increased 50 times (going from 160 $mAh \cdot g^{-1}$ @ 20 $mA \cdot g^{-1}$ to 60 $mAh \cdot g^{-1}$ @ 1,000 $mA \cdot g^{-1}$), demonstrates that these materials can be used in high-power and high-energy Na batteries. The Coulombic efficiency obtained was close to 99% for currents of 50 $mA \cdot g^{-1}$ and above but slightly drops to 98% at 20 $mA \cdot g^{-1}$, possibly due to parasitic reactions occurring at lower currents. It should be noted that the Coulombic efficiency obtained here was also higher compared to what is generally reported ($\approx$95%) for $Ti_3C_2T_z$ MXene electrodes,[3,34] implying that the presence of PC between the layers can reduce parasitic reactions, leading to better Na ions utilization from the cathode.

Finally, to show the effectiveness of our method in preventing water contamination while using MXenes in water sensitive applications, XPS spectra of sodium metal foils exposed to MXenes synthesized using different protocols was analyzed (Figure 6). Briefly, MXene, etched in a solution of HF and water was dried and later dispersed in PC (PC + MX-HF). This dispersion was drop cast on a clean Na foil inside a glove box and excess solvent was allowed to dry out in the glovebox antechamber under vacuum. Similarly, MXene etched and dispersed in PC (PC-MX) was also drop cast on a clean Na foil and dried as above (complete synthesis protocol of both PC-MX and PC + HF-MX and their naming scheme is given in the Experimental Procedures). Both samples, along with a clean Na foil with no coating, were transferred to the XPS without exposing them to air. The Na 1s peak observed around 1,071.2eV in the PC-MX samples (Figure 6, blue) corresponds to metallic sodium Na^0 and does not shift when compared to clean Na metal (Figure 6, black). On the other hand, in the PC + HF-MX samples, the peak is observed at 1,072.3 eV, which corresponds to Na_2O and NaF. This implies that even trace amounts of water in the samples can heavily degrade the surfaces of Na metal. Auger Ti LMM peaks are also observed in the MXene-coated sodium foils as marked in Figure 6. These peaks were used to confirm that the XPS spectra were collected from areas of foil coated with MXene. The severe oxidation of Na surface, even due to trace amounts of water, might

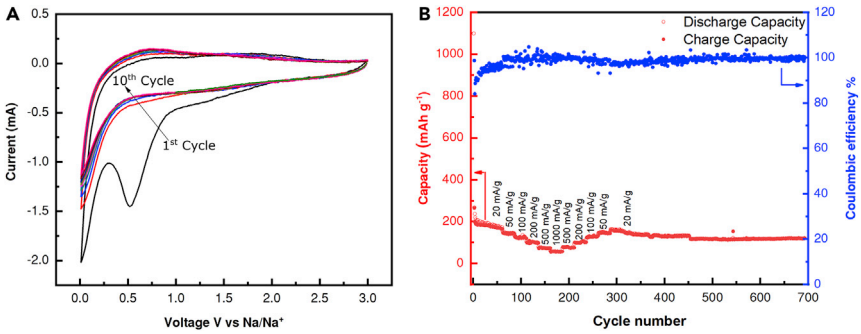

Figure 5. Electrochemical Performance of PC-MX Anodes in Na-Ion Cells

(A) Cyclic voltammograms of cells cycled between 0.01 and 3 V versus Na/Na^+ at 0.2 mV s^{-1}. CV curves of the first 10 cycles are shown.

(B) Cycling performance at a current density of 100 mA g^{-1} and rate performance at current densities of 20, 50, 100, 200, 500, and 1,000 mA g^{-1}. The Coulombic efficiency at the first cycles of every current are not plotted for better representation.

also be one of the reasons why the capacity of the PC-MX electrodes is higher than electrodes of MXene synthesized in water.

Conclusions

In conclusion, we show that it is possible to etch Ti_3AlC_2, in a number of NH_4HF_2-containing polar organic solvents. This method was developed based on the hypothesis that NH_4HF_2 dissociates into NH_4F and HF when dissolved in the polar solvents used herein.[37] The dissolved HF then, most probably, plays the same role it does in water mixtures. This comment notwithstanding, more work is needed to understand the details of the etching mechanism. Several other MAX phases have been converted to their respective MXenes using HF/water as etchant. Based on the results in this work, it is fair to assume that those other MAX phases can most likely also be etched using the method described herein, expanding the scope of MXene applications even further.[2]

This method allows for the whole synthesis to be carried out in a glove box, if needed, which was not possible previously as water was mainly used as a solvent. The result is a highly fluorinated MXene, that has been theorized to have significantly different optical, electronic, and catalytic properties, compared to O-rich terminations obtained when water is the etching medium.[38,39] Electrodes made with PC-$Ti_3C_2T_z$ showed nearly twice the capacity compared to water etched MXene, when tested as anodes in a Na-ion battery.

Lastly, the use of low-boiling-point solvents, like acetonitrile, for etching, can make it easy to recover and purify the solvent for reuse, which can prove to be an important factor when considering industrial-scale MXene synthesis.

EXPERIMENTAL PROCEDURES

MAX Powders

The Ti_3AlC_2 powders were made by mixing titanium carbide, TiC, (Alfa Aesar, 99.5%, 2 μm), aluminum (Alfa Aesar, 99.5%, -325 mesh), and Ti (Alfa Aesar, 99.5%, -325 mesh) powders in a molar ratio of 2:1.05:1, respectively. The mixed powders were ball milled (US Stoneware) for 24 h at 70 rpm and then transferred to an alumina, Al_2O_3, boat, which was placed inside an alumina tube furnace and heated under

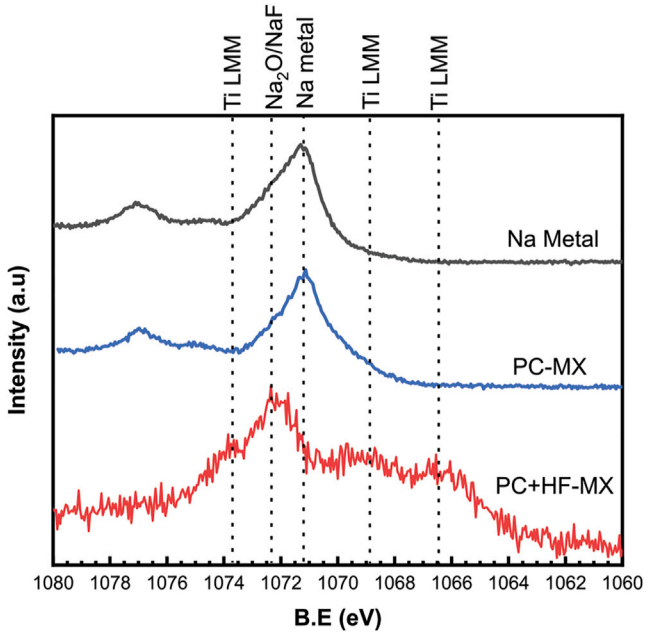

Figure 6. XPS Spectra of Na 1s Region of Na Metal Foil (Black), Na Metal Foil Coated with PC-MX (Blue), and Na Metal Foil Coated with PC + HF-MX

flowing argon (Ar) (flow rate 15 SSCM) to 1,450°C and held at that tempertaure for 2 h. The heating and cooling rates were set at 5°C/min. The resulting loosely sintered blocks were ground, using a milling bit on a drill press. The milled powders were passed through a 400 mesh (particle size < 38 μm) sieve for further experiments. The as-sieved Ti_3AlC_2 powders were transferred to an Ar filled glovebox, for further use.

Etching

Figure 1 is a schematic of the etching, washing, and film formation procedures used in this work when the solvent was PC. It is important to note that this schematic is just that, i.e., it is not intended to show what is actually occurring between, or occupying, the layers. Similar etching procedures were repeated with the other organic solvents listed below. To etch the MAX phase, 1 g of Ti_3AlC_2 was added to 10 mL of the PC (99.7%, anhydrous, Sigma Aldrich USA) to which 1 g of dehydrated NH_4HF_2 (95%, remainder NH_4F, Alfa Aesar, USA) was added. This mixture was stirred, at 500 rpm, inside an Ar-filled glove box for 196 h at 35°C. The first set of XRD patterns (Figures 2A and 2B) were taken after this step.

Washing

The following washing step was necessary to remove the reaction by-products. The slurry obtained above was transferred to an empty 50 mL centrifuge tube and taken out of the glove box for further washing. The remaining volume of the centrifuge tube was then filled with 6 M HCl solution in 2-propanol (>99%, Fisher Scientific, USA), shaken using a vortex mixer for 60 s and centrifuged at 3,500 rpm for 120 s. The resulting clear supernatant was discarded, a fresh acidic propanol solution was added, and the same steps as above were repeated for a total of 5 times. After this step PC was added to the MXene sediment and the tube shaken, using a vortex mixture for 60 s to homogenize the mixture, and again centrifuged at 3,500 rpm for 120 s, after which the clear supernatant was discarded. This process was also repeated a total of 5 times.

Delamination

To delaminate the $Ti_3C_2T_z$ MLs, into single, to few layers, 30 mL of PC was added to the $Ti_3C_2T_z$ slurry and the mixture was sonicated under flowing Ar for 1 h while immersed in an ice bath. The so-formed suspension was centrifuged at 3,500 rpm for 900 s to separate the delaminated $Ti_3C_2T_z$ from the insoluble salts formed during etching and MLs that were not delaminated. The latter process is similar to the one reported by Collini et al. who also used PC as a solvent for delaminating $Ti_3C_2T_z$.[28] During the last centrifugation step, the delaminated MXenes are suspended in the solvent and form a colloid, while the insoluble components like salts produced as etching by-products and heavier particles, like unetched MAX or MXene stacks that did not exfoliate on sonication, are sedimented out.

Film Formation

The supernatant $Ti_3C_2T_z$ colloid was filtered through a Celgard membrane using a mechanical vacuum pump. The filtered film, FF, was vacuum dried overnight powdered using a mortar and pestle and stored in vials under Ar for further analysis. We note that all these procedures were carried out in the ambient atmosphere. The second set of XRD diffraction patterns (Figures 2C and 2D) were taken after this step.

Similar etching and washing procedures as described above were repeated for other solvents including—all obtained from Sigma Aldrich, USA—DXN (99%, anhydrous), ACN (99.8%, anhydrous), DMF (99.8%, anhydrous), DMSO (>99.9%, anhydrous), and NMP (99.5%, anhydrous).

Solvent Exchange

In an attempt to shed some light on the resulting interlayer spacings observed after etching in the polar solvents, we decided to etch Ti_3AlC_2 in HF first and carry out a solvent exchange. To this effect, first 1 g of Ti_3AlC_2 MAX was added to 10 mL of 10% solution of HF in water. This mixture was stirred overnight for 12 h, after which the slurry was decanted into a 50 mL centrifuge tube, and DI water was added to fill the remaining volume. The centrifuge tube was then sealed and shaken for 60 s before centrifuging it at 3,500 rpm for 60 s. The clear acidic supernatant was discarded and DI water was added again, and the washing procedure was repeated until the pH of the supernatant reached $\approx$ 7. After the last washing step, the supernatant was discarded, and the sedimented MXene was collected and air dried.

Lastly, 200 mg of the air-dried powder was added to 40 mL of one of the organic solvents listed above. The bottle was then sealed with parafilm and the mixture stirred for 1 week at room temperature, RT. After stirring, the mixture was again transferred to a centrifuge tube and centrifuged at 3,500 rpm for 60 s, the clear organic solvent supernatant was discarded and the MXene sediment was immediately used for XRD analysis. This HF etched MXene is henceforth labeled as HF-MX. After the solvent exchange the labels are, ACN + HF-MX, DMF + HF-MX etc.

It is important to point out here that care should be taken when working with HF and NH_4HF_2. All the work should be carried out under fume hoods or inside a glove box. Use of HF-resistant personal protection equipment is also necessary. For handling HF and NH_4HF_2 solutions, glassware should be avoided, and high-density polypropylene containers should be used instead.

Characterization

X-ray diffraction (XRD) patterns were acquired on a diffractometer (Rigaku Miniflex, Tokyo, Japan) using Cu K_α radiation (40 kV and 40 mA) with a step size of 0.02° and dwell time of 1.5 s, in the 1.5°–65° 2θ range.

A SEM (Zeiss Supra 50VP, Germany) with an inlens detector and 30 μm aperture was used to examine the morphology and obtain micrographs of the samples.

To collect XPS spectra, Al-Kα X-rays with a spot size of 200 μm and pass energy of 23.5 eV were used to irradiate the sample surface. A step size of 0.5 eV was used to gather the high-resolution spectra. CasaXPS Version 23.19PR1.0 software was used for spectra analysis. The XPS spectra were calibrated by setting the valence edge to zero, which was calculated by fitting the valence edge with a step down function and setting the intersection to 0 eV. Because MXenes are electrically conductive, all MXene peaks were fit using an asymmetric Lorentzian line shape. The background was determined using the Shirley algorithm, which is a built-in function in the CasaXPS software.

To analyze individual MXene flakes, a TEM (JEOL 2100 LaB_6, Tokyo, Japan) was used in bright-field mode. The accelerating voltage was set to 200 kV. To prepare TEM samples, a colloid drop was cast onto a lacy carbon coated copper grid (Cu-400LC, Pacific Grid-Tech) and dried under vacuum.

Zeta Potential measurements were carried out using a NanoBrook Omni (Brookhaven Instruments Corporation, Long Island, NY) system. Colloids were placed inside a quartz cuvette, which was loaded inside the machine. Each sample was allowed to stabilize for 30 s before measurement. Three measurements were taken for each sample, and data were then averaged. The zeta potential values were obtained using the Smoluchowski equation, taking into consideration the viscosity and dielectric constant of the organic solvent used.

To prepare our electrodes, the PC-MX powder was mixed with Super P Conductive carbon (Alfa Aesar, USA) and polyvinylidene fluoride (PVDF) (MTI chemicals, USA) binder in a weight ratio of 70:20:10 in nominal NMP (TCI, USA). This slurry was then cast on an Al foil using a doctor blade and dried in a vacuum oven overnight at 40°C to evaporate the NMP. Circular disc electrodes (Ø 11 mm) were punched out and CR-2032 coin cells were assembled in the Ar filled glove box. Sodium, Na, metal served as both counter and reference electrodes. Ethylene carbonate (EC):PC (1:1 v/v), with 5% fluoroethylene carbonate (FEC) with 1M $NaClO_4$ salt dissolved in it was used as the electrolyte. In all cases, the electrodes were cycled between 0.01 and 3 V versus Na/Na^+. For all the electrochemical results shown herein, the capacity was normalized by the weight of the MXene only.

SUPPLEMENTAL INFORMATION

Supplemental Information can be found online at https://doi.org/10.1016/j.chempr.2020.01.019.

ACKNOWLEDGMENTS

We would like to thank Dr. Steven Wrenn and Martin Walsh for their help with zeta potential measurements. This work was funded by the Division of Materials Research of NSF (DMR 1740795).

AUTHOR CONTRIBUTIONS

V.N. and M.W.B. developed the project. V.N. carried out the synthesis. R.P. and V.K. helped with the electrochemical measurements. M.S. helped with SEM and TEM analysis. M.C. helped with the experiments and analysis. All authors helped with writing the manuscript.

DECLARATION OF INTERESTS

The authors declare no competing interests.

Received: November 11, 2019
Revised: January 13, 2020
Accepted: January 24, 2020
Published: February 24, 2020

REFERENCES

1. Naguib, M., Kurtoglu, M., Presser, V., Lu, J., Niu, J., Heon, M., Hultman, L., Gogotsi, Y., and Barsoum, M.W. (2011). Two-dimensional nanocrystals produced by exfoliation of Ti_3AlC_2. Adv. Mater. *23*, 4248–4253.

2. Verger, L., Xu, C., Natu, V., Cheng, H.-M., Ren, W., and Barsoum, M.W. (2019). Overview of the synthesis of MXenes and other ultrathin 2D transition metal carbides and nitrides. Curr. Opin. Solid State Mater. Sci. *23*, 149–163.

3. Natu, V., Clites, M., Pomerantseva, E., and Barsoum, M.W. (2018). Mesoporous MXene powders synthesized by acid induced crumpling and their use as Na-ion battery anodes. Mater. Res. Lett. *6*, 230–235.

4. Intikhab, S., Natu, V., Li, J., Li, Y., Tao, Q., Rosen, J., Barsoum, M.W., and Snyder, J. (2019). Stoichiometry and surface structure dependence of hydrogen evolution reaction activity and stability of Mo_xC MXenes. J. Catal. *371*, 325–332.

5. Kim, S.J., Koh, H.J., Ren, C.E., Kwon, O., Maleski, K., Cho, S.Y., Anasori, B., Kim, C.K., Choi, Y.K., Kim, J., et al. (2018). Metallic $Ti_3C_2T_x$ MXene gas sensors with ultrahigh signal-to-noise ratio. ACS Nano *12*, 986–993.

6. Ying, Y., Liu, Y., Wang, X., Mao, Y., Cao, W., Hu, P., and Peng, X. (2015). Two-dimensional titanium carbide for efficiently reductive removal of highly toxic chromium(VI) from water. ACS Appl. Mater. Interfaces *7*, 1795–1803.

7. Carey, M., Hinton, Z., Sokol, M., Alvarez, N.J., and Barsoum, M.W. (2019). Nylon-6/$Ti_3C_2T_z$ MXene nanocomposites synthesized by in situ ring opening polymerization of ϵ-caprolactam and their water transport properties. ACS Appl. Mater. Interfaces *11*, 20425–20436.

8. Shahzad, F., Alhabeb, M., Hatter, C.B., Anasori, B., Man Hong, S., Koo, C.M., and Gogotsi, Y. (2016). Electromagnetic interference shielding with 2D transition metal carbides (MXenes). Science *353*, 1137–1140.

9. Sokol, M., Natu, V., Kota, S., and Barsoum, M.W. (2019). On the chemical diversity of the MAX phases. Trends Chem. *1*, 210–223.

10. Rackl, T., Eisenburger, L., Niklaus, R., and Johrendt, D. (2019). Syntheses and physical properties of the MAX phase boride Nb_2SB and the solid solutions $Nb_2SB_xC_{1-x}$(x = 0–1). Phys. Rev. Mater. *3*, 054001.

11. Naguib, M., Unocic, R.R., Armstrong, B.L., and Nanda, J. (2015). Large-scale delamination of multi-layers transition metal carbides and carbonitrides "MXenes". Dalton Trans. *44*, 9353–9358.

12. Ghidiu, M., Lukatskaya, M.R., Zhao, M.Q., Gogotsi, Y., and Barsoum, M.W. (2014). Conductive two-dimensional titanium carbide 'clay' with high volumetric capacitance. Nature *516*, 78–81.

13. Li, T., Yao, L., Liu, Q., Gu, J., Luo, R., Li, J., Yan, X., Wang, W., Liu, P., Chen, B., et al. (2018). Fluorine-free synthesis of high-purity $Ti_3C_2T_x$ (T=OH, O) via alkali treatment. Angew. Chem. Int. Ed. *57*, 6115–6119.

14. Yang, S., Zhang, P., Wang, F., Ricciardulli, A.G., Lohe, M.R., Blom, P.W.M., and Feng, X. (2018). Fluoride-free synthesis of two-dimensional titanium carbide (MXene) using a binary aqueous system. Angew. Chem. Int. Ed. *57*, 15491–15495.

15. Li, M., Lu, J., Luo, K., Li, Y., Chang, K., Chen, K., Zhou, J., Rosen, J., Hultman, L., Eklund, P., et al. (2019). Element replacement approach by reaction with lewis acidic molten salts to synthesize nanolaminated MAX phases and MXenes. J. Am. Chem. Soc. *141*, 4730–4737.

16. Natu, V., Sokol, M., Verger, L., and Barsoum, M.W. (2018). Effect of edge charges on stability and aggregation of $Ti_3C_2T_z$ MXene colloidal suspensions. J. Phys. Chem. C *122*, 27745–27753.

17. Vicic, D.A., and Jones, G.D. (2007). Experimental methods and techniques: basic techniques. In Comprehensive Organometallic Chemistry III (Elsevier), pp. 197–218.

18. Isac-García, J., Dobado, J.A., Calvo-Flores, F.G., and Martínez-García, H. (2016). Microscale. In Experimental Organic Chemistry (Elsevier), pp. 353–370.

19. Laufersky, G., Bradley, S., Frécaut, E., Lein, M., and Nann, T. (2018). Unraveling aminophosphine redox mechanisms for glovebox-free InP quantum dot syntheses. Nanoscale *10*, 8752–8762.

20. Xu, K. (2014). Electrolytes and interphases in Li-Ion batteries and beyond. Chem. Rev. *114*, 11503–11618.

21. Ghidiu, M., and Barsoum, M.W. (2017). The {110} reflection in X-ray diffraction of MXene films: misinterpretation and measurement via non-standard orientation. J. Am. Ceram. Soc. *100*, 5395–5399.

22. Halim, J., Lukatskaya, M.R., Cook, K.M., Lu, J., Smith, C.R., Näslund, L.A., May, S.J., Hultman, L., Gogotsi, Y., Eklund, P., and Barsoum, M.W. (2014). Transparent conductive two-dimensional titanium carbide epitaxial thin films. Chem. Mater. *26*, 2374–2381.

23. Verger, L., Natu, V., Ghidiu, M., and Barsoum, M.W. (2019). Effect of cationic exchange on the hydration and swelling behavior of $Ti_3C_2T_z$ MXenes. J. Phys. Chem. C *123*, 20044–20050.

24. Ghidiu, M., Halim, J., Kota, S., Bish, D., Gogotsi, Y., and Barsoum, M.W. (2016). Ion-exchange and cation solvation reactions in Ti_3C_2 MXene. Chem. Mater. *28*, 3507–3514.

25. Olejnik, S., Posner, A.M., and Quirk, J.P. (1970). The intercalation of polar organic compounds into kaolinite. Clay Miner. *8*, 421–434.

26. Gardolinski, J.E., Peralta-Zamora, P., and Wypych, F. (1999). Preparation and characterization of a Kaolinite-1-methyl-2-Pyrrolidone intercalation compound. J. Colloid Interface Sci. *211*, 137–141.

27. Voigt, C.A., Ghidiu, M., Natu, V., and Barsoum, M.W. (2018). Anion adsorption, $Ti_3C_2T_z$ MXene multilayers, and their effect on claylike swelling. J. Phys. Chem. C *122*, 23172–23179.

28. Collini, P., Kota, S., Dillon, A.D., Barsoum, M.W., and Fafarman, A.T. (2017). Electrophoretic deposition of two-dimensional titanium carbide (MXene) thick films. J. Electrochem. Soc. *164*, D573–D580.

29. Maleski, K., Mochalin, V.N., and Gogotsi, Y. (2017). Dispersions of two-dimensional titanium carbide MXene in organic solvents. Chem. Mater. *29*, 1632–1640.

30. Halim, J., Cook, K.M., Naguib, M., Eklund, P., Gogotsi, Y., Rosen, J., and Barsoum, M.W. (2016). X-ray photoelectron spectroscopy of

select multi-layered transition metal carbides (MXenes). Appl. Surf. Sci. *362*, 406–417.

31. Zhao, M.Q., Xie, X., Ren, C.E., Makaryan, T., Anasori, B., Wang, G., and Gogotsi, Y. (2017). Hollow MXene spheres and 3D macroporous MXene frameworks for Na-Ion storage. Adv. Mater. *29*, 1702410.

32. Zhao, D., Clites, M., Ying, G., Kota, S., Wang, J., Natu, V., Wang, X., Pomerantseva, E., Cao, M., and Barsoum, M.W. (2018). Alkali-induced crumpling of $Ti_3C_2T_x$ (MXene) to form 3D porous networks for sodium ion storage. Chem. Commun. (Camb.) *54*, 4533–4536.

33. Lukatskaya, M.R., Bak, S.-M., Yu, X., Yang, X.-Q., Barsoum, M.W., and Gogotsi, Y. (2015). Probing the mechanism of high capacitance in 2D titanium carbide using in situ X-ray absorption spectroscopy. Adv. Energy Mater. *5*, 1500589.

34. Kajiyama, S., Szabova, L., Sodeyama, K., Iinuma, H., Morita, R., Gotoh, K., Tateyama, Y., Okubo, M., and Yamada, A. (2016). Sodium-ion intercalation mechanism in MXene nanosheets. ACS Nano *10*, 3334–3341.

35. Kurra, N., Alhabeb, M., Maleski, K., Wang, C.-H., Alshareef, H.N., and Gogotsi, Y. (2018). Bistacked titanium carbide (MXene) anodes for hybrid sodium-ion capacitors. ACS Energy Lett. *3*, 2094–2100.

36. Lin, Z., Barbara, D., Taberna, P.-L., Van Aken, K.L., Anasori, B., Gogotsi, Y., and Simon, P. (2016). Capacitance of $Ti_3C_2T_x$ MXene in ionic liquid electrolyte. J. Power Sources *326*, 575–579.

37. Aigueperse, J., Mollard, P., Devilliers, D., Chemla, M., Faron, R., Romano, R., et al. (2000). Fluorine compounds, inorganic. In Ullmann's Encyclopedia of Industrial Chemistry (Wiley-VCH), pp. 398–435.

38. Li, S., Tuo, P., Xie, J., Zhang, X., Xu, J., Bao, J., Pan, B., and Xie, Y. (2018). Ultrathin MXene nanosheets with rich fluorine termination groups realizing efficient electrocatalytic hydrogen evolution. Nano Energy *47*, 512–518.

39. Berdiyorov, G.R. (2016). Optical properties of functionalized $Ti_3C_2T_2$ (T = F, O, OH) MXene: first-principles calculations. AIP Adv. *6*, 055105–055107.